Nonstoichiometry, Structure, and Electrical Properties of "$SrPrO_3$"

Mary A. Thundathil,[†] Camille Y. Jones,[‡] G. Jeffrey Snyder,[§] and Sossina M. Haile*[,†]

Materials Science, California Institute of Technology, Pasadena, California 91125, NIST Center for Neutron Research, National Institute of Standards and Technology, Gaithersburg, Maryland 20899-8562, and Jet Propulsion Laboratory, California Institute of Technology, Pasadena, California 91109

Received April 27, 2005. Revised Manuscript Received June 29, 2005

The single-phase composition with the perovskite structure type in the Sr−Pr−O system has been identified as $(Sr_{0.935}Pr_{0.043}\square_{0.022})Pr_{1.0}O_3$ from neutron diffraction refinements, chemical analysis, and thermogravimetric analysis. The cation deficient oxide crystallizes in a $GdFeO_3$-type orthorhombic structure, space group *Pbnm*, with lattice parameters $a = 5.988\ 00(17)$, $b = 6.121\ 36(17)$, $c = 8.548\ 58(24)$ Å, and $Z = 4$ at 300 K. Thermogravimetric analysis confirms that the compound is not oxygen deficient. $(Sr_{0.935}Pr_{0.043})Pr_{1.0}O_3$ exhibits semiconducting behavior. The bulk (grain interior) conductivity at 36 °C is 5.2×10^{-5} S cm^{-1} with an activation energy for charge transport of 0.26 eV.

Introduction

As part of an ongoing program to develop proton and mixed proton and electron conducting perovskites for application in electrochemical devices, we have examined the properties of $SrPrO_3$. On the basis of an analogy to compounds such as $SrCeO_3$ and $BaCeO_3$,[1,2] acceptor doped $SrPrO_3$ might be anticipated to adsorb atmospheric H_2O and exhibit good proton conductivity, whereas the variable valence of the Pr ion, between the 3+ and 4+ oxidation states, might be anticipated to result in high electronic conductivity. In addition, $SrPrO_3$ and the analogous perovskite $BaPrO_3$ are unusual in their ability to host Pr primarily (if not entirely) in the 4+ oxidation state and have, therefore, been of interest for their magnetic properties.[3−8]

Outside of a few magnetic studies, experimental investigations of $SrPrO_3$ have been limited, and even the crystal structure is in dispute (Table 1). Gramsch and Morss,[9] as part of a general study on the thermochemical properties of $A^{2+}B^{4+}O_3$ (A = Ba, Sr; B = Ce, Pr, Tb) perovskites, prepared $SrPrO_3$ and indexed the X-ray powder diffraction pattern on the basis of an orthorhombic unit cell. This cell is characterized by a $\sqrt{2}a_p \times 2\sqrt{2}a_p \times 2a_p$ distortion, where a_p (≈4 Å) represents the ideal perovskite unit cell parameter. In contrast, Hinatsu and coworkers[10] have indexed the unit cell as a $GdFeO_3$ type perovskite, with a $\sqrt{2}a_p \times \sqrt{2}a_p \times 2a_p$ distortion (also orthorhombic). In both cases, the ideal stoichiometry was assumed. Horyn et al.[11] studied phase formation in the Bi−Pr−Sr−O system and reported the single-phase perovskite to have composition $(Sr_{0.9}Pr_{0.1})PrO_{2.93}$ and a monoclinic crystal structure.

We have undertaken the present work to resolve the discrepancies regarding the structure and stoichiometry of $SrPrO_3$, as well as to determine its electrical properties. Chemical analysis, X-ray and neutron powder diffraction, and thermal analysis have all been employed to provide a conclusive evaluation of the cation occupancies on the A and B sites and of the type of distortion exhibited by this material from the cubic ABO_3 aristotype.

Synthesis and Phase Formation

It became clear during the course of this work that a single perovskite phase in the Sr−Pr−O system resulted only from highly specific stoichiometries that were somewhat deficient in Sr (Sr/Pr < 1). Accordingly, all samples were prepared by chemical solution routes to ensure both the desired stoichiometry and overall homogeneity. Unless stated otherwise, the acrylamide gelation route[12] was employed, a

* Author for correspondence. E-mail: smhaile@caltech.edu. Fax: (626) 395-8868.
[†] Materials Science, California Institute of Technology.
[‡] National Institute of Standards and Technology.
[§] Jet Propulsion Laboratory, California Institute of Technology.

(1) Uchida, H.; Maeda, N.; Iwahara, H. *Solid State Ionics* **1983**, *11*, 117.
(2) Taniguchi, N.; Hatoh, K.; Niikura, J.; Gamo, T.; Iwahara, H. *Solid State Ionics* **1992**, *53−56*, 998.
(3) Jacobson, A. J.; Tofield, B. C.; Fender, B. E. F. *Acta Crystallogr., Sect. B* **1972**, *28*, 956.
(4) Hinatsu, Y. *J. Solid State Chem.* **1993**, *102*, 362.
(5) Rosov, N.; Lynn, J. W.; Lin, Q.; Cao, G.; O'Reilly, J. W.; Pernambuco-Wise, P.; Crow, J. E. *Phys. Rev. B* **1992**, *45*, 982.
(6) Fukui, T.; Ohara, S.; Kawatsu, S. *J. Power Sources* **1998**, *71*, 164.
(7) Cao, G.; Yuen, T.; Pernambuco-Wise, P.; Crow, J. E.; O'Reilly, J. W.; Kuric, M. V.; Guertin, R. P.; Rosov, N.; Lynn, J. W. *J. Appl. Phys.* **1991**, *70*, 6332.
(8) Felner, I.; Yeshurun, Y.; Hilscher, G.; Holbubar, T.; Schaudy, G.; Yaron, U.; Cohen, O.; Wolfus, Y.; Yacoby, E. R.; Klein, L.; Potter, F. H.; Rastomjee, C. S.; Egdell, R. G. *Phys. Rev. B* **1992**, *46*, 9132.
(9) Gramsch, S. A.; Morss, L. R. *J. Chem. Thermodyn.* **1995**, *27*, 551.
(10) (a) Itoh, M.; Hinatsu, Y. *J. Alloys Compd.* **1988**, *264*, 119. (b) Hinatsu, Y.; Itoh, M.; Edelstein, N. *J. Solid State Chem.* **1996**, *132*, 337. Note: The structural data presented in ref 10a,b are contradictory and in each case internally inconsistent. For example, in (a) the space group setting, lattice parameters, and atomic coordinates are consistent with one another; however, the reported bond lengths and angles are inconsistent with the resulting structure. In (b) the space group is given as *Pbnm* for $b > a > c$, but this choice of lattice constants corresponds to setting *Pnma*, while the reported atomic coordinates are consistent with the given setting of *Pbnm*. Apparently, the space group setting, lattice parameters, and atomic coordinates are reported correctly in (a), whereas the bond distances and angles are reported correctly in (b).
(11) Horyn, R.; Wolcyrz, M.; Bukowski, Z. *J. Solid State Chem.* **1996**, *124*, 176.
(12) Douy, A.; Odier, P. *Mater. Res. Bull.* **1989**, *24*, 1119.

10.1021/cm050895k CCC: $30.25
Published on Web 08/31/2005

Table 1. Reported Unit Cell Data for $SrPrO_3$

formula	distortion[a]	space group or crystal class	cell parameters, Å or deg	ref
$SrPrO_3$	$\sqrt{2}a_p \times 2\sqrt{2}a_p \times 2a_p$	orthorhombic	$a = 5.97(1)$ $b = 12.22(1)$ $c = 8.53(1)$	9
$SrPrO_3$	$\sqrt{2}a_p \times \sqrt{2}a_p \times 2a_p$	*Pbnm* (No. 62)[b]	$a = 5.9857(7)$ $b = 6.1168(8)$ $c = 8.5487(9)$	10
$(Sr_{0.9}Pr_{0.1})Pr_1O_{2.93}$	$\sqrt{2}a_p \times \sqrt{2}a_p \times 2a_p$[c]	monoclinic	$a = 5.9797$ $b = 6.1297$ $c = 8.5617$ $\theta = 90.073$	11

[a] a_p is the equivalent lattice parameter of the ideal cubic perovskite, ~4Å. [b] Transformed from the reported setting of *Pnma*. [c] Presumed on the basis of the reported cell parameters.

technique in which rapid solution gelation occurs and, thus, cation segregation (due, for example, to differential solubilities) is minimized.

Stoichiometric amounts of $Sr(NO_3)_2$ (99.9%, Alfa Aesar) and Pr_6O_{11} (99.9%, Alfa Aesar) were dissolved separately in hot concentrated nitric acid and then mixed together. The mixed metal ion solution was poured into a solution of ethylenediamine tetraacetic acid, or EDTA (99.4+%, Alfa Aesar), dissolved in dilute ammonium hydroxide. Dissolution was achieved by continuous stirring at ~80 °C. The metal ion:EDTA mole ratio was 1:1. To this solution were added acrylamide (99%, Alfa Aesar) and *N*,*N*′-methylene-bis-acrylamide (99+%, Alfa Aesar) dissolved in water by stirring. For 1 mol of $SrPrO_3$, 15 mol of acrylamide, and 0.7 mol of bis-acrylamide were used. To this were then added 2,2′-azobisisobutyronitrile (or AIBN, 98% Aldrich), 0.05 mol per 1 mol of $SrPrO_3$, dissolved in ethanol, and tetramethylethylenediamine (99% Invitrogen), 18.2 mL per 1 mol of $SrPrO_3$, to initiate polymerization. Greenish gels were obtained within minutes. Most of the organic components in the gel were removed by heating to 450 °C in air for 12 h. The decomposed product was finely ground and calcined at 900 °C in oxygen. To establish the precise stoichiometry at which the single-phase perovskite could be obtained, samples with Sr:Pr ratios of $(1 - x):(1 + x)$ were prepared, where x was varied from 0 to 0.1 in increments of 0.05.

For comparative purposes, Sr_2PrO_4[13] was also synthesized, in this case using a modified Pechini process.[14] Stoichiometric amounts of $Sr(NO_3)_2$ and Pr_6O_{11} were again dissolved in nitric acid, and EDTA was used as the chelating agent but with a metal ion:EDTA mole ratio of 1:2. To this chelated solution was then added 0.5 mol of ethylene glycol. Polymerization of the organic components occurred upon heating to 80 °C, at which the solution was held overnight. The gel was decomposed at 250 °C, and the resulting powder annealed under oxygen at 500 °C for 2 h and at 950 °C for 2 h. The calcined powder was finely ground and annealed in O_2 at 1050 °C for 2 h and then furnace-cooled to room temperature.

Phase evolution was examined by X-ray powder diffraction (Siemens D-500, Cu Kα radiation, 0.01° steps, 15 s/step). The patterns obtained from stoichiometric $SrPrO_3$ and from Sr_2PrO_4 are compared in Figure 1. At first glance, the stoichiometric material appears single-phase. That is, because

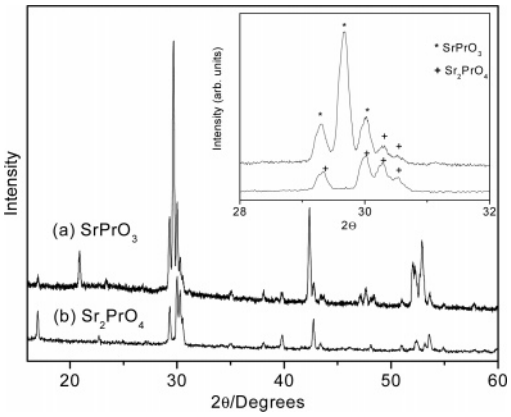

Figure 1. Comparison of powder X-ray diffraction patterns of (a) stoichiometric $SrPrO_3$ and (b) Sr_2PrO_4. The additional (non-perovskite) peaks in the pattern of $SrPrO_3$ clearly correspond to Sr_2PrO_4 (inset).

of the overlap in the positions of the high-intensity peaks of Sr_2PrO_4 with that of the perovskite phase, it is easy to overlook the presence of Sr_2PrO_4 in samples of $SrPrO_3$. If the very weak Sr_2PrO_4 peaks at $2\theta \sim 17$, 30.3, and 30.5° are disregarded (see Figure 1, inset), the pattern obtained from $SrPrO_3$ can be indexed on the basis of a $GdFeO_3$-type[15] orthorhombic perovskite with lattice parameters similar to those reported by Itoh and Hinatsu.[10] Those authors similarly observed additional peaks in their diffraction pattern, reported to occur at $2\theta \sim 15°$ and at $2\theta \sim 30°$, which could not be indexed on the basis of the selected perovskite cell. Alternatively, if the weak peak at $2\theta \sim 17°$ is (incorrectly) taken into consideration while those at $2\theta \sim 30.4°$ (which appear only as a slight shoulder to the main perovskite peak at ~30° under more typical data collection conditions) are ignored, the same pattern can be indexed on the basis of an orthorhombic cell with lattice constants $a = 5.97$ Å, $b = 12.21$ Å, and $c = 8.53$ Å, as proposed by Gramsch and Morss.[9] Longo et al.[16] earlier indexed $SrCeO_3$ on a similar cell, and this was later found by others to be incorrect.[17,18] Thus, the presence of Sr_2PrO_4 in nominally single-phase $SrPrO_3$ perovskite is responsible for the discrepancies in the literature.

The X-ray patterns obtained from the $Sr_{1-x}Pr_{1+x}O_{3\pm\delta}$ series of materials are shown in Figure 2. As the Sr/Pr ratio was decreased from 1 (i.e., as x was increased), the concentration

(13) Fiscus, J. E.; Loye, H. Z. *J. Alloys Compd.* **2000**, *306*, 141.
(14) Agarwal, V.; Liu, M. L. *J. Mater. Sci.* **1997**, *32*, 619.
(15) Geller, S. *J. Chem. Phys.* **1956**, *24*, 1236.
(16) Longo, V.; Ricciardiello, F.; Minichelli, D. *J. Mater. Sci.* **1981**, *16*, 3503.
(17) Knight, K. S.; Bonanos, N. *Mater. Res. Bull.* **1995**, *30*, 347.
(18) Ranlov, J.; Lebech, B.; Nielsen, K. *J. Mater. Chem.* **1995**, *5*, 743.

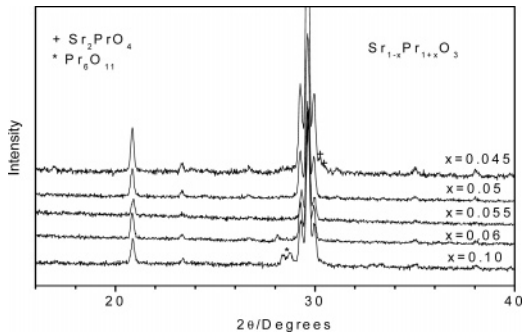

Figure 2. Powder X-ray diffraction patterns of $Sr_{1-x}Pr_{1+x}O_{3\pm\delta}$ showing the emergence of the single-phase perovskite for composition $Sr_{0.945}Pr_{1.055}O_{3\pm\delta}$.

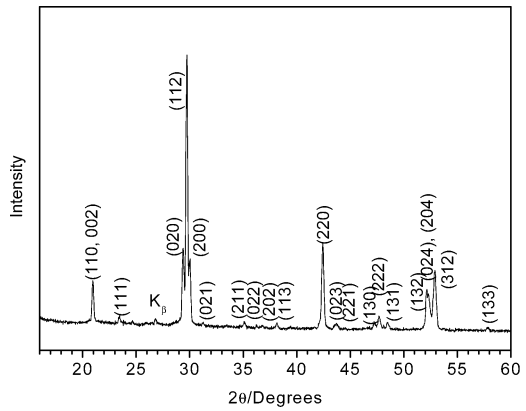

Figure 3. Powder X-ray diffraction pattern of single-phase "$SrPrO_3$" obtained from a starting composition of $Sr_{0.945}Pr_{1.055}O_{3\pm\delta}$. Peaks are indexed on the basis of an orthorhombic cell.

of the Sr_2PrO_4 phase decreased. Careful examination of the patterns shows that the $x = 0.055$ phase is devoid of peaks attributable to Sr_2PrO_4 and of any other impurity phases detectable by X-ray diffraction. A further increase of the Pr content resulted in the formation of Pr_6O_{11} as a minor phase. Thus, the composition of the single-phase perovskite is identified as $Sr_{0.945}Pr_{1.055}O_{3\pm\delta}$. The $Sr_{0.9}Pr_{1.1}O_3$ composition, reported by Horyn et al.[11] as monoclinic, single-phasic perovskite, yields a two-phase mixture in our studies ($x =$ 0.1 in Figure 2), but the general observation of those authors that the perovskite phase contains excess Pr is in agreement with our results. The as-prepared single-phase $Sr_{0.945}Pr_{1.055}O_{3\pm\delta}$ is light green in color. Its X-ray pattern, indexed on the basis of an orthorhombic cell with lattice parameters $a = 5.9870(6)$ Å, $b = 6.1232(6)$ Å, and $c = 8.5515(8)$ Å, is shown in Figure 3.

Chemical Analysis

The phase evolution studies showed clearly that the perovskite phase "$SrPrO_3$" exists over a narrow compositional range (Sr/Pr ratio) and that single-phase formation results from samples with nominal stoichiometry $Sr_{0.945}Pr_{1.055}O_{3\pm\delta}$ (Sr/Pr = 0.896). The reliability and accuracy of this result was investigated by chemical analysis of both the starting materials, $Sr(NO_3)_2$ and Pr_6O_{11}, and the product perovskite phase. In addition, the oxygen content, which provides a measure of the Pr oxidation state (and thereby indications of site occupancy), was determined by thermogravimetric analysis.

Experimental Details. Elemental analysis was performed by inductively coupled plasma−mass spectroscopy (ICP-MS, Hewlett-Packard 4500). Six different sample solutions, with concentrations ranging between 0.05 and 0.25 ppm by mass of Sr and Pr, were prepared by dissolving $Sr_{0.945}Pr_{1.055}O_{3\pm\delta}$ (100 mg to 200 mg) in 1% HNO_3 (100 mL) and further diluting to the desired concentrations. These solutions were introduced into the ICP-MS, and the resultant Sr and Pr signals (m/z = 44 and 47, respectively) converted into concentrations using previously measured calibration curves. Each solution was measured 10 times. The calibration scales were determined by dilution (to six different levels between 0.05 and 0.25 ppm by mass) of standard solutions of Sr and Pr in 1% HNO_3. Measurements of the standard solutions were also performed 10 times each. Samples from three different batches of calcined, single-phase perovskite were evaluated. The metal contents in the starting materials, $Sr(NO_3)_2$ and Pr_6O_{11}, were analyzed in a similar manner. Six different solutions, containing 0.05−0.25 ppm by mass of Sr and Pr, were prepared by dissolving 200−420 mg of $Sr(NO_3)_2$ and 150−200 mg of Pr_6O_{11}, respectively, in 1% HNO_3 (100 mL) and further diluting to the desired concentrations.

Thermal analysis was carried out by heating single-phasic $Sr_{0.945}Pr_{1.055}O_{3\pm\delta}$ powder (21.3 mg) to 1100 °C (Netzsch STA 449 C) at a rate of 20 °C/min under 4% H_2/96% argon. X-ray diffraction of the products showed only Pr_2O_3 and $SrCO_3$ to be present post-reduction (the carbonate is formed as a result of SrO reaction with atmospheric CO_2 after removal from the thermal analyzer), permitting quantitative analysis of the results.

Results. The elemental analysis showed the Sr/Pr ratio of the single-phase material to be 0.925 ± 0.010, whereas the metals contents in the starting materials were found to be 96.6 ± 0.8 % and 96.1 ± 1.0%, respectively, of the expected values. The implied input Sr/Pr ratio for the single-phase material based on the analysis of the starting materials is 0.912 ± 0.022. The two sets of chemical analyses (of product material and of input chemicals) suggest that the Sr content might be slightly higher than the nominal value (Sr/Pr = 0.896) but, nevertheless, clearly confirm that the Sr/Pr ratio is significantly less than 1. Given that the nominal stoichiometry and the two sets of chemical analysis results are all within two standard deviations of one another, we use, for ease, the nominal stoichiometry, $Sr_{0.945}Pr_{1.055}O_{3\pm\delta}$, in the subsequent discussion.

The relative mass of the single-phase perovskite as a function of temperature is shown in Figure 4. The observed mass change upon complete reduction over the temperature range 200−900 °C is 2.90 wt %. A weight loss of 0.06% that occurs at lower temperatures is attributed to the removal of moisture from the surface of the powder. Because the synthesis was carried out under oxidizing atmospheres, the Pr^{2+} concentration is assumed to be negligible and the decomposition of $Sr_{0.945}Pr_{1.055}O_{3\pm\delta}$ (Sr/Pr = 0.896) can be written as

$$[Sr_{0.896}O_{0.896}]PrO_{2-\delta} \rightarrow 0.896SrO + {}^1/_2Pr_2O_3 + ({}^1/_4 - \delta/2)O_2 \quad (1)$$

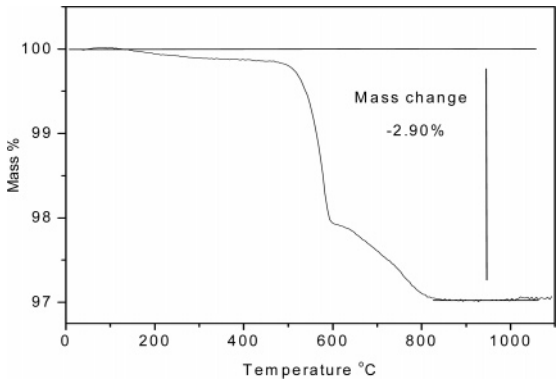

Figure 4. Weight change of single-phase "$SrPrO_3$" under 4% H_2/96% argon. Thermogravimetric analysis data collected at a heating rate of 20 K/min.

where fractional occupancies at the A and B sites of the perovskite structure are not meant to be implied. From a weight change of 2.90%, the value of δ is 0.019, and the oxygen content per formula unit as written in eq 1 is 2.877. From a $2 - \delta$ value of 1.981, the concentration of Pr in the 3+ oxidation state is 3.8% and the chemical formula of the single-phase perovskite can then be written as "$Sr_{0.896}Pr^{3+}_{0.038}Pr^{4+}_{0.962}O_{2.877}$", where, again, fractional site occupancies are not meant to be implied.

Structural Analysis

The overall stoichiometry obtained for single-phase perovskite, "$Sr_{0.896}Pr^{3+}_{0.038}Pr^{4+}_{0.962}O_{2.877}$" or simply "$SrPrO_3$", suggests either mixed cation occupancy on the A site or a substantial vacancy concentration on that site (or some combination of these effects). Furthermore, the distribution of cations on the A and B sites must be connected to the concentration (if any) of anion vacancies. To explicitly determine the cation and anion site occupancies, neutron powder diffraction experiments were performed on "$SrPrO_3$" at 300 and 80 K. Data were collected on the BT-1 32-detector neutron powder diffractometer at the NIST Center for Neutron Research.[19,20] The instrument settings were a Cu(311) monochromator with a wavelength of 1.5398 Å, a takeoff angle of 90°, and in-pile collimation of 15 min of arc. The beam was masked to 1.59 × 5.08 cm at the sample. Measurements were made on ~6.5 g of sample in a vanadium can of length 5.08 cm and inner diameter of 1.56 cm. Data were collected over the range of $3° < 2\theta < 167°$ with a step size of 0.05° 2θ, with the $3-5° 2\theta$ range omitted from the refinement.

Preliminary analysis showed that both the room temperature and 80 K sample adopt the orthorhombic perovskite structure, indicating the absence of any phase transitions over this temperature range. Because the occupancy factor and thermal displacement parameters of any atom are highly correlated and because low temperatures minimize thermal vibrations, the 80 K structure was refined first, and the site occupancies obtained from that analysis were applied to the 300 K structure. The data collected at 80 K contained Al peaks originating from the closed-cycle refrigerator and, thus, the corresponding 2θ ranges were omitted from the refinement (40−40.75, 44.4−45.1, 64.95−65.75, 116.75−117.55, 137.55−139.2, >160°).

Refinement at 80 K. The structure was refined in space group *Pbnm* (No. 62) with $a \approx < b < c$ and $Z = 4$. Unlike the case for $BaPrO_3$ and $BaCeO_3$, in which the two shorter lattice constants are almost equal in length (differing by less than 0.03 Å or 0.5%), there is no difficulty in properly assigning the lattice constants in "$SrPrO_3$" relative to the selected space group setting. That is, the structures of both barium compounds were initially reported in space group *Pbnm* with $a \approx < b < c$[3] and later with the *a* and *b* parameters interchanged.[5,17,21] In the case of the cerate, the correction has been made explicitly,[21] whereas in the case of $BaPrO_3$ the two conflicting structure reports originate from different laboratories[3,5] and the question of proper assignment of the lattice parameters has not yet been entirely resolved. In the present study of "$SrPrO_3$", refinements in which the *a* and *b* axes were interchanged resulted in dramatic worsening of the refinement statistics and were not pursued. Refinement of the structural model was performed using the GSAS[22] program operated under EXPGUI[23] software and using the atomic parameters reported in ref 10a as the starting point. Neutron scattering lengths were taken from ref 26. For convenience, only Sr, with variable occupancy, was placed on the A site (4c), and from the refined occupancy the relative Sr, Pr, and vacancy concentrations were later calculated.

The least-squares refinement included lattice parameters, diffractometer zero, background parameters (14-term Chebyshev polynomial function), and peak profiles (GSAS function 1: u, v, w, asym). In the initial stages, each of the positional parameters, fractional occupancies, and isotropic thermal parameters were refined independently and successively updated in subsequent cycles. Attempts to simultaneously refine the occupancies and thermal parameters of anions were (not surprisingly) unsuccessful. Refinement of oxygen site occupancies with fixed thermal parameters did not show significant deviations from 1, and, hence, these occupancies were fixed at unity for the remainder of the analysis. The isotropic refinement of the structure converged to a χ^2 of 1.6 for 28 variables. The Sr occupancy at the A site refined to a value of 0.959(6). The Pr occupancy at the B site refined to full occupancy.

Anisotropic refinement of all atoms led to an improvement of χ^2, and, hence, the anisotropic model was retained. In the final stages, all the positional parameters, anisotropic atomic displacement parameters for all atoms, and fractional occupancies for the cations together with the various background and profile parameters were simultaneously refined.

(19) The instrument is described in the NCNR website. http://www.ncnr.nist.gov/ (accessed 2005).
(20) Certain commercial materials are identified in this paper to foster understanding. Such identification does not imply recommendation or endorsement by the National Institute of Standards and Technology, nor does it imply that the materials identified are necessarily the best available for the purpose.
(21) Knight, K. S.; Bonanos, N. *J. Mater. Chem.* **1994**, *4*, 899.
(22) Larson, A. C.; Von Dreele, R. B. *General Structure Analysis System*; LAUR 86-748; Los Alamos National Laboratory: Los Alamos, NM, 1994.
(23) Toby, B. H. *J. Appl. Crystallogr.* **2001**, *34*, 210.

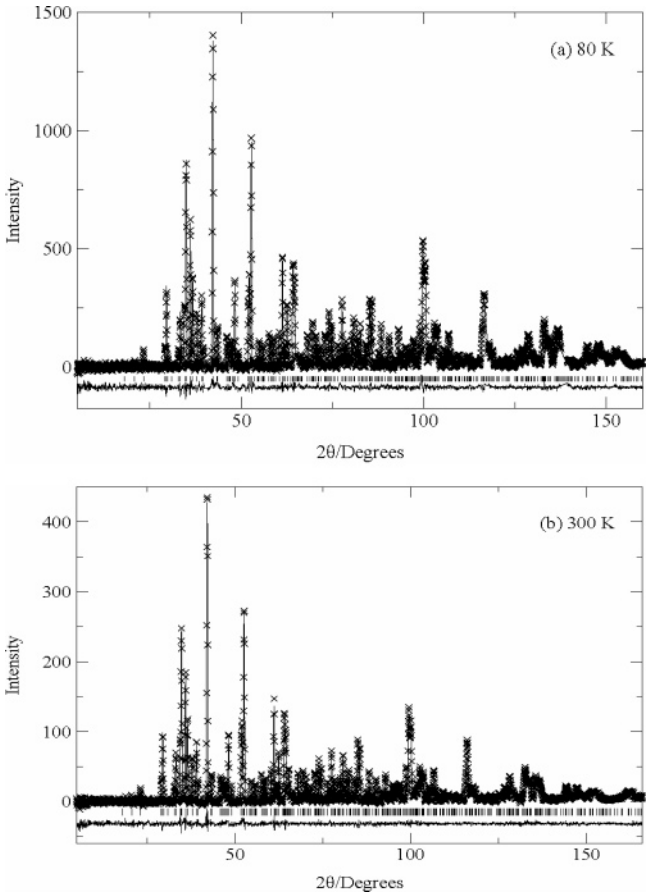

Figure 5. Rietveld refinement of powder neutron diffraction data recorded at (a) 80 K and (b) 300 K for "$SrPrO_3$". Observed (cross), calculated (line), and difference (bottom) profiles are shown. Tick marks represent expected peak positions.

Table 2. Crystal Data and Structure Refinement Parameters for $Sr_{0.945}Pr_{1.055}O_3$ ("$SrPrO_3$") at 80 and 300 K

	80 K	300 K
space group	*Pbnm* (No. 62)	*Pbnm* (No. 62)
a (Å)	5.9747(2)	5.9880(2)
b (Å)	6.1188(2)	6.1214(2)
c (Å)	8.5325(2)	8.5486(2)
Z	4	4
V (Å)	311.93(2)	313.35(2)
$R_p \times 100$	3.14	3.02
$R_{wp} \times 100$	3.97	3.59
$R_F^2 \times 100$	4.96	3.31
χ^2	1.37	1.29

The Sr occupancy at the A site refined to 0.963(6) whereas the Pr occupancy (at the B site) refined to 1.000(7). The final refinement converged to a $\chi^2 = 1.37$ for 367 reflections and 52 variables. The unit cell data and structure refinement parameters are given in Table 2. The observed and fitted neutron diffraction profiles are shown in Figure 5a, and a thermal ellipsoid representation of a portion of the crystal structure is shown in Figure 6a.

Turning to the question of site occupancies in "$SrPrO_3$", several scenarios for accommodating the chemical formula "$Sr_{0.896}Pr^{3+}_{0.038}Pr^{4+}_{0.962}O_{2.877}$" (as obtained from the chemical and thermal analyses) within the perovskite structure are possible. Those which involve (i) Pr^{2+} ions (at either the A or the B sites), (ii) Pr^{4+} at the A site, (iii) anion or cation interstitials, or (iv) B-site vacancies are all immediately ruled out for crystal chemical reasons. Under these constraints,

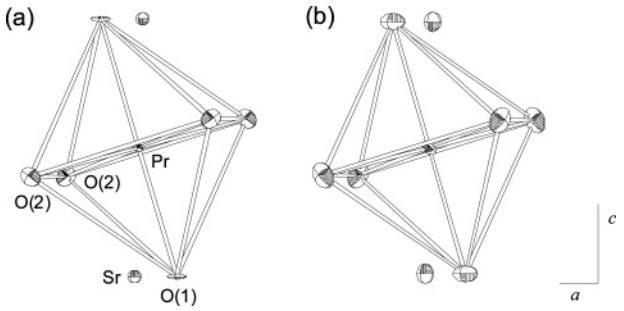

Figure 6. Thermal ellipsoid representation of a PrO_6 group centered at $^1/_2 00$ in the structure of "$SrPrO_3$", shown in projection on (010): (a) 80 K and (b) 300 K. For simplicity, the A-site atom has been labeled as "Sr"; however, this site is occupied by both Sr and Pr and additionally contains substantial vacancies.

the only manner in which a Sr/Pr ratio of less than 1 can be accommodated is via the incorporation of Pr^{3+} cations on the A site and/or a significant vacancy content (Sr deficiency) on that site. Other species which must also, in principle, be considered for overall charge neutrality requirements are anion vacancies and Pr^{3+} cations on the B site. Thus, the relevant species are X_{Sr} (fractional Sr occupancy on the A site), $X_{Pr^{4+}}$ (fractional Pr^{4+} occupancy on the B site), $X_{Pr_A{}^{3+}}$ (fractional Pr^{3+} occupancy on the A site), $X_{Pr_B{}^{3+}}$ (fractional Pr^{3+} occupancy on the B site), and X_O (the mean oxygen occupancy on the anion sites). The elemental chemical analysis, the thermal analysis, and the neutron diffraction analysis yield the following relationships between these parameters.

The elemental analysis implies

$$\frac{X_{Sr}}{X_{Pr^{4+}} + X_{Pr_A{}^{3+}} + X_{Pr_B{}^{4+}}} = 0.896 \quad (2)$$

whereas the thermogravimetric analysis implies

$$\frac{X_{Pr_A{}^{3+}} + X_{Pr_B{}^{3+}}}{X_{Pr^{4+}}} = \frac{3.80}{96.2} \quad (3)$$

From the observation that the oxygen site occupancies are all 1, and the requirement of overall charge balance, one obtains

$$3X_O = 3 = 2X_{Pr^{4+}} + (3/2)X_{Pr_A{}^{3+}} + (3/2)X_{Pr_B{}^{3+}} + X_{Sr} \quad (4)$$

while the full occupancy at the B site implies

$$X_{Pr^{4+}} + X_{Pr_B{}^{3+}} = 1 \quad (5)$$

The Sr occupancy obtained at the A site, 0.963, implies a total scattering length from this site of $0.963 \times 7.02 = 6.763$ barns (where the scattering length of strontium is 7.02 barns). Assuming mixed Sr/Pr occupancy on the A site, this total scattering length can be expressed as the average of the Sr and Pr scattering lengths (4.58 barns for the latter), weighted according to their respective occupancies, X_{Sr} and $X_{Pr_A{}^{3+}}$:

$$7.02X_{Sr} + 4.58X_{Pr_A{}^{3+}} = 6.763 \quad (6)$$

Solving eqs 2−4 for $X_{Pr^{4+}}$ yields a value of 0.997. (Using a Sr/Pr value of 0.925, as determined from the chemical

Table 3. Atomic Coordinates And Thermal Displacement Parameters of $Sr_{0.945}Pr_{1.055}O_3$ ("$SrPrO_3$") at 80 and 300 K[a]

temp	atom	*x*	*y*	*z*	site occupancy	U_{11}	U_{22}	U_{33}	U_{12}	U_{13}	U_{23}
80 K	Sr	−0.0112(2)	0.0462(0)	1/4	0.963(6)	0.56(7)	0.63(6)	0.49(6)	−0.18(6)	0	0
	Pr	0	1/2	0	1.000(7)	0.25(10)	0.54(10)	0.16(8)	−0.26(8)	0.04(9)	−0.10(5)
	O1	0.1051(3)	0.4568(3)	1/4	1.00	1.13(7)	0.82(6)	0.08(7)	−0.09(6)	0	0
	O2	0.7007(2)	0.2986(2)	0.0563(1)	1.00	1.10(5)	0.70(5)	1.04(5)	−0.29(5)	0.21(5)	−0.19(4)
300 K	Sr	−0.0103(3)	0.0435(2)	1/4	0.963	1.01(6)	0.97(5)	1.22(6)	−0.27(6)	0	0
	Pr	0	1/2	0	1.00	0.56(9)	0.90(8)	0.51(7)	−0.15(8)	0.19(9)	0.02(5)
	O1	0.1029(3)	0.4582(3)	1/4	1.00	1.70(7)	1.49(7)	0.67(7)	−0.19(6)	0	0
	O2	0.7007(2)	0.2986(2)	0.0547(2)	1.00	1.42(5)	1.32(5)	1.99(6)	−0.60(5)	0.42(5)	−0.50(5)

[a] The estimated standard deviation in the final digit is given in parentheses. Anisotropic temperature factors are of the form $\exp[-2\pi^2(h^2u_{11}a^{*2} + ... + hku_{12}a^*b^* + ...)]$ and are given in units of 10^{-2} Å^2. The compound crystallizes in space group *Pbnm* and has lattice constants $a = 5.9747(2)$, $b = 6.1188(2)$, and $c = 8.5325(2)$ Å at 80 K.

analysis of the single-phase perovskite, yields a value of $X_{Pr^{4+}}$ of 1.005.) Thus, to the accuracy of our estimation, the B site in "$SrPrO_3$" is fully and exclusively occupied by Pr^{4+} ions. Such a result is consistent with the fact that the Sr^{2+} ion the A site is relatively small and, thus, large species such as Pr^{3+} on the B site are not favored. With $X_{Pr^{4+}} = 1$ and $X_{Pr_B^{3+}} = 0$, eq 4 simplifies to

$$3X_{Pr_A^{3+}} + 2X_{Sr} = 2 \quad (7)$$

which, together with eq 6, yields a molecular formula for the single-phase "$SrPrO_3$" perovskite of $(Sr_{0.935}Pr_{0.043}\square_{0.022})$-$Pr_{1.0}O_3$.

Overall, the strontium to praseodymium molar ratio, Sr/Pr, of 0.90 obtained from neutron diffraction refinement is precisely the nominal value, which, as stated above, is in good agreement with the Sr/Pr ratio of 0.925(10) obtained from ICP analysis. It should be noted, however, that the final chemical formula as written here implies that 4.3% of the Pr is in the 3+ oxidation state. This differs slightly from the thermal analysis value of 3.9% because of the $X_{Pr^{4+}}$ value of 0.997 having been approximated as 1.

Refinement at 300 K. As described previously, refinement of the structural model at 300 K was performed with the site occupancies of all atoms fixed at the values obtained at low temperature. All other structural and profile parameters were varied, including anisotropic thermal parameters for all atoms. The unit cell data and structure refinement parameters are given in Table 2. The anisotropic refinement converged to a χ^2 value of 1.29. The agreement factors are better for the 300 K refinement than for that of 80 K, primarily because the data did not contain any extra peaks from Al. The observed and fitted neutron diffraction profiles are shown in Figure 5b, and a thermal ellipsoid representation of a portion of the crystal structure is shown in Figure 6b.

Structural Features of "$SrPrO_3$". The values for the refined coordinates, fractional occupancies, and anisotropic displacement parameters for cations and anions are given in Table 3, for the 80 and 300 K measurements. There are statistically significant differences in the derived structural quantities (bond lengths and angles) from those reported in ref 10b, which we attribute to the utilization of neutrons in the present work in contrast to the X-ray methods used in the earlier work.

Although the defect chemistry of "$SrPrO_3$" is highly unusual, its structural chemistry is less so. Its perovskite structure is formed from rather regular PrO_6 polyhedra, arranged with a $GdFeO_3$-type orthorhombic distortion, Figure 7. The magnitude of the deviation of the B−O−B bond angle from 180° in an ABO_3 perovskite provides a measure of the extent of octahedral tilting relative to its orientation in the ideal cubic perovskite.[24] The Pr−O−Pr angles measured here, 143.34(8) and 147.33(6)°, indicate that the tilting is rather large, being much greater than that observed in $BaPrO_3$ (∼174°)[3,5] and comparable to that in $SrCeO_3$ (∼145°),[18] both of which also crystallize as $GdFeO_3$-type perovskites. The extent of orthorhombic distortion can be expressed in terms of the fractional difference between the "equivalent" lattice parameters, $c/\sqrt{2}$ and a (where the unit cell distortion is of the type $\sqrt{2}a_p \times \sqrt{2}a_p \times 2a_p$ with c as the longest axis). For zero octahedral tilting, $a = c/\sqrt{2}$[3]. By this measure as well, $SrPrO_3$ exhibits a distortion (5.8%) that is comparable to that of $SrCeO_3$ (6.1%)[18] and much greater than that of $BaPrO_3$ (1.4%).

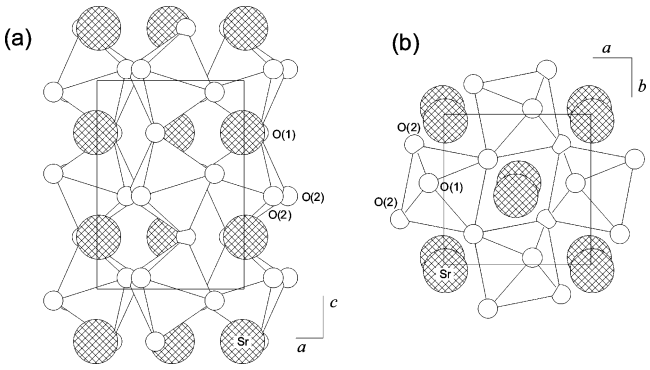

Figure 7. Structure of "$SrPrO_3$" shown in projection (a) on (010) and (b) on (001).

Cooling produces slight but detectable changes in the structure of "$SrPrO_3$". Overall, the structure contracts along all three axes, with higher contraction occurring along the a direction and corresponding to an increase in the orthorhombic distortion. The coefficients of the linear thermal expansion (α) over the temperature range 80−300 K along the axes a (α_a), b (α_b), and c (α_c) are 9.87×10^{-6}/°C, 1.85×10^{-6}/°C and 8.52×10^{-6}/°C, respectively. The corresponding coefficient of volume thermal expansion β ($\beta = \alpha_a + \alpha_b + \alpha_c$) is 20.24×10^{-6}/°C. The contraction on cooling is primarily due to a decrease in the Sr−O bond lengths, which decrease in average value from 2.749 to 2.739 Å. In contrast, the temperature change has little impact on the PrO_6 octahedron, which remains regular in shape and has an unchanged Pr−O distance of 2.234 Å.

(24) Glazer, A. M. *Acta Crystallogr., Sect. B* **1972**, *28*, 3384.

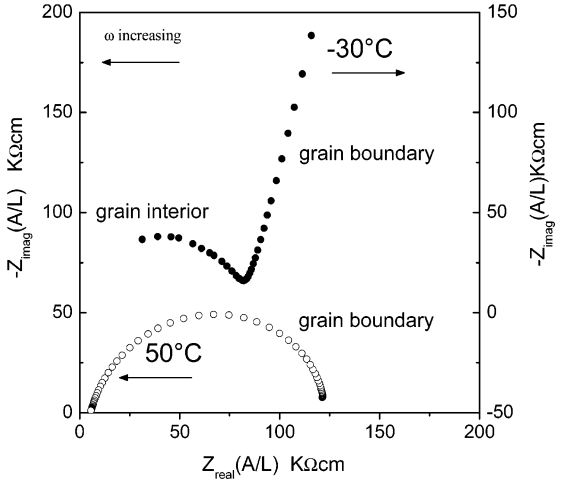

Figure 8. Nyquist impedance plots obtained from "$SrPrO_3$" at 50 °C and −30 °C, as indicated.

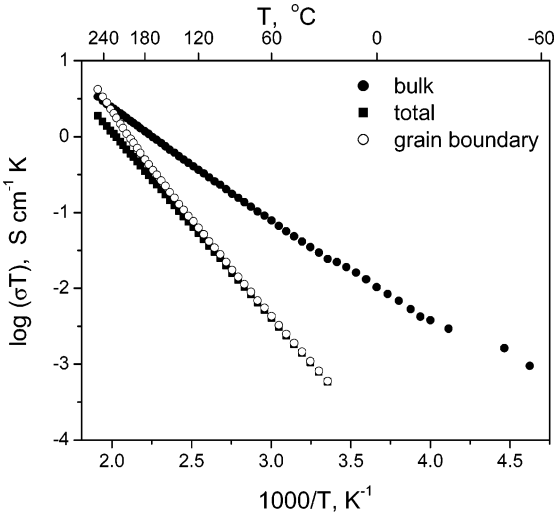

Figure 9. Conductivity of "$SrPrO_3$" as a function of temperature, presented in Arrhenius form.

Electrical Properties

Samples of single-phase "$SrPrO_3$" for electrical characterization were prepared from powders calcined at 950 °C. Powders were uniaxially pressed under 452 MPa and subsequently sintered at 1050 °C in oxygen to yield pellet samples 8.3 mm in diameter and 9 mm in thickness. The density, as estimated from the mass and geometrical dimension of the pellets, was 5.3 g/cm^3 (∼91% of theoretical). Sintering under laboratory air or at higher temperatures resulted in decomposition of the material into a multicomponent mixture containing, in addition to the majority perovskite phase, Pr_6O_{11}, Sr_2PrO_4, and $SrCO_3$ (with the carbonate presumably having been formed from the reaction of the product SrO with laboratory CO_2 in the period between decomposition and X-ray analysis).

Electrical conductivity was measured by alternating current impedance spectroscopy over the frequency range 20 Hz to 1 MHz with an applied voltage of 1 V (HP 4284A-LCR analyzer). Opposite sides of the sample were coated with silver metal paste to serve as electrodes. Data were collected over the temperature range −57 to 250 °C in air. Frequency-dependent impedance data were fit to an equivalent circuit model using the commercial least squares refinement program ZView 2.[25] The Seebeck coefficient was measured in vacuum using a light-pipe technique described elsewhere[26] and W−Nb thermocouples. The same disc-shaped sample utilized for conductivity measurements was employed for these experiments. As a result of the high resistance of the sample at low temperatures and the instability of the material in vacuum at high temperatures, reliable Seebeck coefficient data were obtained only in a narrow temperature range of 460 °C < T < 590 °C.

Nyquist impedance plots ($-Z_i$ vs Z_r representation) obtained at 50 and −30 °C are presented in Figure 8. At temperatures above 45 °C, the spectra consist of a single semicircular arc, which corresponds to the grain boundary response. At 50 °C the characteristic frequency of this arc (frequency at the peak of the arc) is 1.0×10^4 Hz implying an effective capacitance of 4.62×10^{-9} F, which, in turn, implies a relative dielectric constant, >8600, that is too large to be associated with bulk behavior. Instead, the high-frequency displacement of this arc from the origin is taken as the bulk resistance. At temperatures below 0 °C, the high-frequency semicircular arc corresponding to the bulk response is clearly evident. In particular, at −30 °C, the characteristic frequency, capacitance, and relative dielectric constant are 5.13×10^6 Hz, 1.25×10^{-11} F, and 29.3, respectively, consistent with bulk behavior.

The conductivity is plotted in Arrhenius form, log(σT) verses 1000/T, in Figure 9. The bulk, grain boundary, and total conductivity are all shown. The bulk conductivity of "$SrPrO_3$" obeys Arrhenius behavior, with an activation energy of 0.27 eV. The activation energy (E_a) for charge transport across grain boundaries is 0.52 eV, and the transport process is, again, quite Arrhenius in behavior. The grain boundary conductivity has not been normalized for grain size effects[27] because of the limited temperature regime over which both bulk and grain boundary arcs could be measured. Nevertheless, it can be concluded, simply from the existence of a grain boundary arc,[27] that the grain boundaries in "$SrPrO_3$" serve as high resistance barriers to charge transport rather than high conductivity pathways, presumably as a result of electron scattering at these interfaces. Overall, the conduction process in the polycrystalline sample of "$SrPrO_3$" examined here is dominated by the high resistance grain boundaries to a temperature of ∼140 °C but at higher temperatures begins to exhibit more bulk-like behavior.

The Seebeck coefficient, α, of "$SrPrO_3$" is fairly temperature-independent, Figure 10, with a value of approximately −215 μV/K over the entire temperature range 460−590 °C. The sign of the Seebeck coefficient indicates that the material is an n-type conductor and rules out protons as possible majority carriers, because these, as dilute, dissolved species, would produce a positive Seebeck coefficient. The magnitude of the conductivity of "$SrPrO_3$" at 250 °C is about 1 order of magnitude greater than that of doped $BaCeO_3$, the material with the highest reported proton conductivity, and is, thus,

(25) Johnson, D. *Software ZView-V.2.1b*; Scribner Associates, Inc.: Southern Pines, NC, 1999.
(26) Wood, C.; Zoltan, L. D.; Stapfer, G. *Rev. Sci. Instrum.* **1985**, *56*, 719.
(27) Haile, S. M.; West, D. L.; Campbell, J. *J. Mater. Res.* **1998**, *13*, 1576.

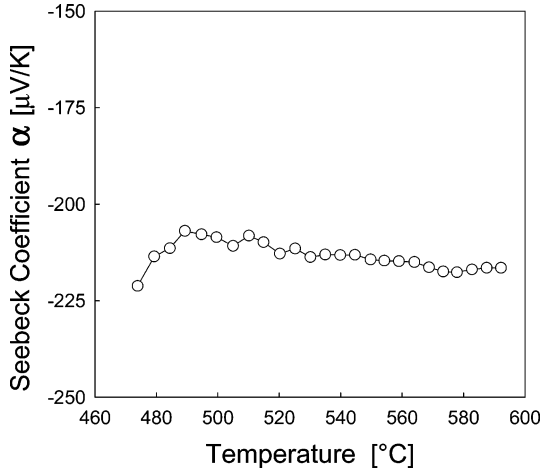

Figure 10. Seebeck coefficient of "$SrPrO_3$" as a function of temperature.

consistent with electronic rather than protonic conduction. Similarly, the much lower activation energy for charge transport supports the conclusion of electronic conduction. In comparison to materials such as $(La_{2/3}Sr_{1/3})MnO_3$ and $(La_{2/3}Ca_{1/3})MnO_3$, however, with similar, thermally activated electronic transport, the conductivity of "$SrPrO_3$" is very low (several orders of magnitude lower) and the activation energy very high [for example, $E_a = 0.073$ eV in $(La_{2/3}Ca_{1/3})MnO_3$].[28]

The existence of free electrons as charge carriers in "$SrPrO_3$" can be understood in terms of charge compensating defects for the Pr^{3+} on the Sr^{2+} site. If compensation is accommodated entirely through the generation of cation vacancies (as implied in the structural discussion), charge balance then requires

$$[Pr_{Sr}{}^{3+}] = 2[V_{Sr}] \tag{8}$$

where the left-hand side represents the concentration of Pr^{3+} cations in the A site and the bracketed quantity on the right-hand side represents the concentration of vacancies on the A site. Under this scenario, the concentration of all other charge-carrying species (oxygen vacancies, electrons, and holes) is negligible. If, however, the concentration of vacancies is slightly lower than the value implied by eq 8, charge balance may be achieved through the generation of electronic defects, as illustrated in eq 9

$$[Pr_{Sr}{}^{3+}] = 2[V_{Sr}] + n \tag{9}$$

where n is the concentration of free electrons. In this manner, incorporation of the higher valence Pr cation onto the A^{2+} site would introduce free electrons into the material, giving rise to the n-type electronic conductivity observed.

The value of the Seebeck coefficient is, in principle, related to the concentration of "free" electron carriers. This relationship is, to first a approximation, embodied in the Heikes formula[29]

$$\alpha = \frac{k_b}{q} \ln\left(\frac{1-c}{c}\right) \tag{10}$$

where k_b is Boltzmann's constant, q is the charge of the carrier, and c is the ionization fraction. The Seebeck coefficient measured here for "$SrPrO_3$" implies $c = 7.5\%$. If one assumes, as is typical of perovskites, that electron transport occurs via the B-site cations, the result effectively implies that 7.5% of the Pr on the B site is in the 3+ valence state, in contradiction to the defect chemical analysis presented above. Factors such as spin entropy contributions to the Seebeck coefficient, repulsive interactions between carriers (both ignored in the Heikes formula),[30] and possible exclusion of B cation sites located in the vicinity of A-site vacancies from the electron transport process may account for this apparent discrepancy.

That "$SrPrO_3$" is n-type may have interesting implications for the possibility of mixed proton electron conduction. Materials such as $BaCeO_3$ are p-type at high temperatures and under atmospheric conditions.[31] Introduction of protons via exposure to hydrogen introduces electrons and thereby lowers the electronic (hole) carrier concentration:

$$^1/_2H_2 + p + O_O \rightarrow OH_O \tag{11}$$

where p is an electronic hole, O_O represents an oxygen ion on an oxygen site, and OH_O represents a hydroxyl group on an oxygen site. For an n-type material, exposure to hydrogen is expected to instead further increase the electronic carrier concentration via

$$Pr_{Pr}{}^{4+} + {}^1/_2H_2 + O_O \rightarrow Pr_{Pr}{}^{3+} (\approx e) + OH_O \tag{12}$$

In this way, high concentrations of both protons and electrons may be attained. Indeed, very high hydrogen contents have been measured in the analogous material $BaPrO_3$.[32]

Discussion: Structure and Stoichiometry

Neutron diffraction refinements established that $Sr_{0.935}Pr_{0.043}Pr_{1.0}O_3$ crystallizes in the $GdFeO_3$-type orthorhombic structure at room temperature, similar to $SrCeO_3$,[17,18] $SrTbO_3$,[33] and $SrZrO_3$.[34] The Pr-containing perovskite differs from these other compounds in that it has mixed ion occupancy at the A site and is slightly cation deficient. A-site vacancies (~2%) serve as the primary charge-compensating defects for Pr^{3+} cations also residing at the A site. Several ABO_3 type perovskite oxides are known to accommodate substantial concentrations of A-site vacancies,[35] and such defects are not uncommon. In contrast, the presence of B-site cations on the A site in $A^{2+}B^{4+}O_3$ perovskites has not been previously reported. The reason for its occurrence in "$SrPrO_3$" is not entirely obvious. There would seem to

(28) Snyder, G. J.; Hiskes, R.; DiCarolis, S.; Beasley, M. R.; Geballe, T. H. *Phys. Rev. B* **1996**, *53*, 14434.
(29) Chaikin, P. M.; Beni, G. *Phys. Rev. B* **1976**, *13*, 647.
(30) Jaime, M.; Salamon, M. B.; Rubinstein, M.; Treece, R. E.; Horwitz, J. S.; Chrisey, D. B. *Phys. Rev. B* **1996**, *54*, 11914.
(31) Iwahara, H.; Uchida, H.; Ono, K.; Ogakik, K. *J. Electrochem. Soc.* **1988**, *135*, 529.
(32) Jones, C. Y.; Wu, J.; Li, L. P.; Haile, S. M. *J. Appl. Phys.* **2005**, *97*, 114908.
(33) Tezuka, K.; Itoh, M.; Haga, M.; Hinatsu, Y. *Mater. Sci. Forum* **1999**, *315−317*, 578.
(34) Howard, C. J.; Knight, K. S.; Kennedy, B. J.; Kisi, E. H. *J. Phys.: Condens. Matter* **2000**, *12*, L677.
(35) Kharton, V. V.; Kovalevsky, A. V.; Tsipis, E. V.; Viskup, A. P.; Naumovich, E. N.; Jurado, J. R.; Frade, J. R. *J. Solid State Electrochem.* **2002**, *7*, 30.

be no structural imperative for replacing the Sr^{2+} ion (1.58 Å in 12-fold coordination) by the smaller Pr^{3+} ion (1.48 Å in 12-fold coordination). An explanation may be found in the electronic behavior of the Pr ion. In the most stable form of praseodymium oxide under ambient conditions, Pr_6O_{11}, Pr exists in both the 3+ and the 4+ oxidation states. Formation of $(Sr_{0.935}Pr_{0.043})Pr_{1.0}O_3$, in which both oxidation states are also present, may represent the most favorable means of achieving mixed $Pr^{3+/4+}$ valence within the perovskite structure. Incorporation of Pr^{3+} on the Sr^{2+} site may introduce smaller local structural distortions than reduction of a portion of the Pr^{4+} on the B site; Pr^{3+} in 8-fold coordination is only 6% smaller than Sr^{2+} (also 8-fold coordination), whereas Pr^{3+} in 6-fold coordination is 14% larger than Pr^{4+} (also in 6-fold coordination).

Conclusions

The chemical formula of the single-phasic perovskite phase in the Sr−Pr−O system is identified by a combination of chemical analysis, thermal analysis, and neutron diffraction refinement as $(Sr_{0.935}Pr_{0.043})Pr_{1.0}O_3$. It is a cation-deficient perovskite with a $GdFeO_3$-type orthorhombic distortion. The bond lengths and angles are well within the range of values expected for Sr- and Pr- containing oxides. There are several key differences between "$SrPrO_3$" and isostructural $BaPrO_3$: (i) $BaPrO_3$ can be prepared in air whereas the Sr analogue requires an oxygen atmosphere, (ii) unlike $BaPrO_3$, single-phasic $SrPrO_3$ exhibits mixed cation occupancy and vacancies at the A site, and (iii) the magnitude of the PrO_6 octahedral tilt and, hence, the orthorhombic distortion are greater in the Sr analogue. The mixed occupancy at the A site may be driven by a combination of the equilibrium between Pr^{4+} and Pr^{3+} under ambient oxygen pressure and a minimization of local structural distortions in the perovskite structure. The conductivity of "$SrPrO_3$" is n-type electronic, which can be explained in terms of charge-compensating defects for Pr^{3+} on the Sr site. If proton transport can additionally be demonstrated in "$SrPrO_3$", this compound or its derivatives may have applicability in hydrogen separation membranes or other electrochemical devices.

Acknowledgment. This work was supported by DOE office of Energy Efficiency and Renewable Energy. The authors gratefully acknowledge the assistance of Dr. Tetsuya Uda with chemical analysis and for valuable discussions.

Supporting Information Available: Complete experimental details and crystallographic parameters resulting from the structrual refinements of "$SrPrO_3$" at 30 and 300 K (CIF). This material is available free of charge via the Internet at http://pubs.acs.org.

CM050895K